Physica A 389 (2010) 1412–1424

Contents lists available at ScienceDirect

Physica A

journal homepage: www.elsevier.com/locate/physa

A model for mesoscale patterns in motile populations

Matthew J. Simpson *, Kerry A. Landman, Barry D. Hughes, Anthony E. Fernando

Department of Mathematics and Statistics, University of Melbourne, Victoria 3010, Australia

ARTICLE INFO

Article history:
Received 4 September 2009
Received in revised form 19 November 2009
Available online 22 December 2009

Keywords:
Cell motility
Chain migration
Aggregation
Exclusion process
Nonlinear diffusion

ABSTRACT

Experimental observations of cell migration often describe the presence of mesoscale patterns within motile cell populations. These patterns can take the form of cells moving as aggregates or in chain-like formation. Here we present a discrete model capable of producing mesoscale patterns. These patterns are formed by biasing movements to favor a particular configuration of agent–agent attachments using a binding function $f(K)$, where K is the scaled local coordination number. This discrete model is related to a nonlinear diffusion equation, where we relate the nonlinear diffusivity $D(C)$ to the binding function f. The nonlinear diffusion equation supports a range of solutions which can be either smooth or discontinuous. Aggregation patterns can be produced with the discrete model, and we show that there is a transition between the presence and absence of aggregation depending on the sign of $D(C)$. A combination of simulation and analysis shows that both the existence of mesoscale patterns and the validity of the continuum model depend on the form of f. Our results suggest that there may be no formal continuum description of a motile system with strong mesoscale patterns.

1. Introduction

Cell migration is a multiscale phenomenon where experimental observations are made over a range of scales depending on the system of interest. For example, macroscopic observations of cell densities are made to characterize the invasiveness of cell populations [1,2], whereas microscopic observations of individual cell trajectories are made to characterize the details of the migration mechanism [3,4]. Observations of cell migration are also made at intermediate scales, which we shall call the mesoscale. These observations correspond to visual patterns that form within a motile population. Two common mesoscale patterns in cell biology include the formation of motile aggregates of cells [5,6], as well as the formation of chain-like patterns [7–9].

Traditional modeling approaches were often interested in describing macroscopic properties of a cell population, such as the spatial distribution of cell densities. For such applications continuum models were appropriate, and various motility mechanisms have been considered [1,2]. Recent advances in microscopy now provide high quality confocal, time-lapse and magnetic resonance imaging data. This new data provides opportunities to develop models at the individual cell level [10].

There is great interest in the correspondence between the discrete and continuum models of cell motility. The starting point can be a spatially discrete, continuous in time, nearest-neighbor master equation for a probability distribution function [11–14]. In the appropriate limits, this gives rise to a partial differential equation (PDE) description of cell density. An alternative approach starts with a spatially and temporally discrete exclusion process with biologically realistic discrete cell motility rules. The spatially and temporally discrete model can be averaged to provide a continuum description of the system [15–17]. This is the approach we take here since the spatially and temporally discrete exclusion process is well suited for the interpretation of time-lapse data.

* Corresponding author. Tel.: +61 3 83446517; fax: +61 3 83444599.
E-mail address: m12.simpson@qut.edu.au (M.J. Simpson).

0378-4371/$ – see front matter © 2009 Elsevier B.V. All rights reserved.
doi:10.1016/j.physa.2009.12.010

Here we describe and analyze a lattice-based discrete motility model which takes account of contacts or binding between agents. Motility events are governed, in part, by a binding function $f(K)$, where $K \in [0, 1]$ is the scaled coordination number of the target site and f is a function that will bias movements to favor a particular coordination number at the target site. The discrete model, based on a simple exclusion process [18], is averaged to give a continuum description of the expected behavior of the system in terms of: (i) a PDE description of the population density [15,18], and (ii) differential equations describing the average trajectory, or pathline, of a tagged agent within the population [16]. Using simulation and visual inspection, we demonstrate that the model can produce a range of mesoscale patterns including chains and aggregates. Different patterns correspond to different choices of $f(K)$ and different initial conditions.

We find that the macroscopic density is governed by a nonlinear diffusion equation. This is an intriguing outcome. Although standard unbiased exclusion processes involve interacting agents, the population-level density obeys a linear diffusion equation, since the interactions are symmetric and do not appear in the continuum model [15,18]. In the discrete model presented here, the discrete interactions are asymmetric and now appear in the continuum description through the nonlinear diffusivity $D(C)$, where C is the continuum density.

The PDE model developed here admits a range of solutions with complex behaviors depending on the form of $D(C)$. In particular, the PDE with appropriate initial conditions admits both smooth and discontinuous solutions, depending on whether $D(C)$ is positive or negative [19,20]. The discrete model can also generate aggregation patterns when the diffusivity is negative. This behavior is related to the backward heat equation [19,21]. This contrasts the discrete exclusion process of Deroulers et al. that accounted for maintaining neighbors and gave rise to a positive nonlinear diffusivity [17].

Our analysis suggests that the formation of strong mesoscale patterns (chains, aggregates) and the validity of the continuum models described here depend on the form of $f(K)$. Furthermore our results suggest that strong mesoscale patterns may not have any continuum description. This means that the application of a continuum model to capture a mesoscale chain-like structure may be inappropriate. Although this study is motivated with examples from cell biology, this work has implications for related applications involving collective migration that include ecological applications [22], malignant invasion [23] and pedestrian motility [24].

2. The discrete model

Simulation data presented in this work will use the two-dimensional square lattice as a specific illustration of the model. However, most of the analysis applies to arbitrary d-dimensional periodic lattices with spacing Δ. Agents can be viewed as occupying sites. Alternatively, agents can be regarded as residing in regions, since each site $\mathbf{s}$ is associated with a spatial region consisting of all points closer to site $\mathbf{s}$ than to any other. In various contexts these regions are known as Voronoi regions or Wigner–Seitz regions [25]. In two dimensions, these regions become polygonal tiles: the square lattice is associated with square tiles, while the triangular lattice is associated with hexagonal tiles.

For any site $\mathbf{s}$ on a periodic lattice, we define two sets of sites:

$\mathcal{N}\{\mathbf{s}\}$ denotes the set of nearest-neighbor sites, that is, those sites one bond distant from $\mathbf{s}$—in the model, these are the sites to which movements from site $\mathbf{s}$ can be attempted;
$\mathcal{A}\{\mathbf{s}\}$ denotes the set of sites whose associated regions have boundaries that touch the boundary associated with site $\mathbf{s}$—in the model, the occupancy of these sites affect motility events that would place an agent at site $\mathbf{s}$.

The numbers of sites in $\mathcal{N}\{\mathbf{s}\}$ and $\mathcal{A}\{\mathbf{s}\}$ are denoted $z_{\mathcal{N}}$ and $z_{\mathcal{A}}$ respectively. For the square lattice, if $\mathbf{s} = (i, j)$, where $i, j \in \mathbb{Z}$, then

$$\mathcal{N}\{(i,j)\} = \{(i-1,j), (i+1,j), (i,j-1), (i,j+1)\},$$
$$\mathcal{A}\{(i,j)\} = \mathcal{N}\{(i,j)\} \cup \{(i+1,j+1), (i+1,j-1), (i-1,j+1), (i-1,j-1)\},$$

and so $z_{\mathcal{N}} = 4$ and $z_{\mathcal{A}} = 8$. For the triangular lattice (hexagonal tiling) $\mathcal{A}\{\mathbf{s}\} = \mathcal{N}\{\mathbf{s}\}$ and $z_{\mathcal{N}} = z_{\mathcal{A}} = 6$.

A simple exclusion process [18,26,27] is realized on the periodic lattice. Each site can be occupied by at most one agent. The occupancy of site $\mathbf{s}$ is $C_{\mathbf{s}}$, with $C_{\mathbf{s}} = 1$ for an occupied site, and $C_{\mathbf{s}} = 0$ for an empty site.

If there are N agents on the lattice, then for each time step of duration τ, we make N sequential independent random choices of an agent. On average, each agent is chosen once per time step. When chosen, an agent attempts to move with probability P. The parameters P and τ together define the motility of an isolated agent, but agents that are close together affect each other's motility as we now explain.

A motile agent at site $\mathbf{s}$ inspects all sites in $\mathcal{N}\{\mathbf{s}\}$, and for each site $\mathbf{s}' \in \mathcal{N}\{\mathbf{s}\}$, the agent associates a scaled local coordination number, or a measure of occupancy of the neighborhood of site $\mathbf{s}'$,

$$K_{\mathbf{s}'} = \frac{1}{z_{\mathcal{A}}} \sum_{\mathbf{s}^* \in \mathcal{A}\{\mathbf{s}'\}} C_{\mathbf{s}^*},$$

so that $K_{\mathbf{s}'} \in [0, 1]$. The scaled local coordination number ranks the potential number of agent–agent attachments that can be made by an agent placed at each target site. The value of $K_{\mathbf{s}'}$ includes the contribution from the motile agent at site $\mathbf{s}$. For example, Fig. 1 illustrates these ideas on the square lattice. The central site $\mathbf{s}'$ in Fig. 1 has three occupied neighboring sites and $K_{\mathbf{s}'} = 3/8$.

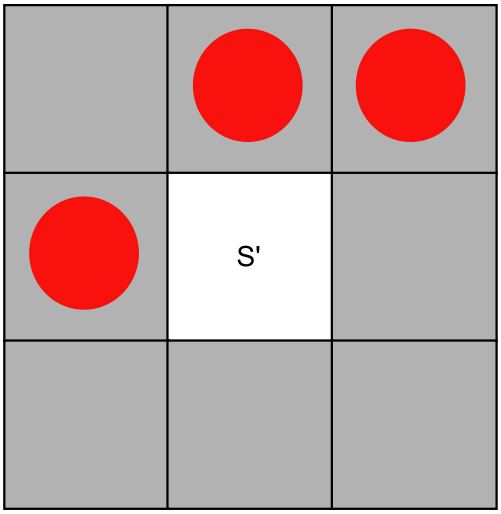

Fig. 1. Schematic representation showing the potential agent–agent bonds that can be formed by an agent moving to site $\mathbf{s}'$. Agents are represented as red circles. The set of sites $\mathcal{A}\{\mathbf{s}'\}$ are shaded grey. Since $z_{\mathcal{A}} = 8$ and three of these sites are occupied $K_{\mathbf{s}'} = 3/8$.

The propensity for movements to any target site is governed by a nonnegative *binding function* $f(K)$, chosen to reflect a particular preference in scaled coordination number. A motile agent at site $\mathbf{s}$ steps to $\mathbf{s}' \in \mathcal{N}\{\mathbf{s}\}$ with probability

$$\frac{f(K_{\mathbf{s}'})}{\sum_{\mathbf{s}'' \in \mathcal{N}\{\mathbf{s}\}} f(K_{\mathbf{s}''})}.$$

Of course, since the model is an exclusion process, attempted movements to sites that are already occupied are aborted.

3. Discrete simulation data: Influence of $f(K)$

To demonstrate the influence of different binding functions, we present a suite of simulations on a two-dimensional square lattice of size 100×100. Periodic boundary conditions are imposed along all boundaries. Initially, each site $(x, y) = (i\Delta, j\Delta)$ with $35 \leq i, j \leq 65$ is occupied with probability 0.5. Snapshots of four simulations, after 200 time steps, are shown in Fig. 2. Results in Fig. 2(a), with $f(K) = 1$, show a symmetric distribution of agents where there is no apparent preference for the local coordination number. This is intuitively reasonable, since selecting a constant binding function means that all movements are independent of the coordination number of the target site and the model becomes a symmetric simple exclusion process [18].

Snapshots in Fig. 2(b)–(c) correspond to $f(K) = \mathrm{e}^{\pm 3K}$. With $f(K) = \mathrm{e}^{-3K}$, we see that movements decreasing the coordination number are favored: the agents are more spread out in Fig. 2(b) compared to Fig. 2(a). Results in Fig. 2(c) clearly illustrate favoring movements to a higher coordination number reflected in the formation of aggregates. Finally, results in Fig. 2(d) correspond to a binding function with a local maximum in $f(K)$ at $K = 0.5$. This means that movements to sites with half the maximum number of neighbors are highly favored over other configurations. We see the effect of this binding function through the chain-like patterns with lacunae.

Results from two cell migration assays are shown in Fig. 2(e)–(f). Data in Fig. 2(e) shows a population of motile ovarian cancer cells [5]. The formation of cell aggregates is an obvious feature of this system. Alternatively, Fig. 2(f) shows the movement of neural precursor cells grown as neurospheres [7]. These cells do not move as discrete units; rather they form distinct chain-like patterns which are also observed within intact tissue cultures [8].

In summary, the four snapshots from the discrete algorithm illustrate that the model can produce a range of behaviors, including the formation of aggregates and chain structures. Some of these patterns are observed in cell migration assays and the mode of cell migration is often described in terms of these mesoscale patterns. For example, the motility mechanism of neural precursor cells is typically described as "chain migration" [8,28]. Of course, we have only shown a limited range of simulations. Further simulations with different $f(K)$ or different initial distributions of agents will produce different results. We will now focus on taking a continuum limit of the discrete motility mechanism. This procedure will establish whether the kinds of mesoscale patterns observed in Fig. 2 can be described with a continuum model.

4. Deriving a continuous description

To connect the discrete mechanism with a continuum model we define the average occupancy of site $\mathbf{s}$, averaged over many statistically identical realizations, as $\langle C_{\mathbf{s}} \rangle$. After averaging, we form a discrete conservation statement describing $\delta\langle C_{\mathbf{s}} \rangle$,

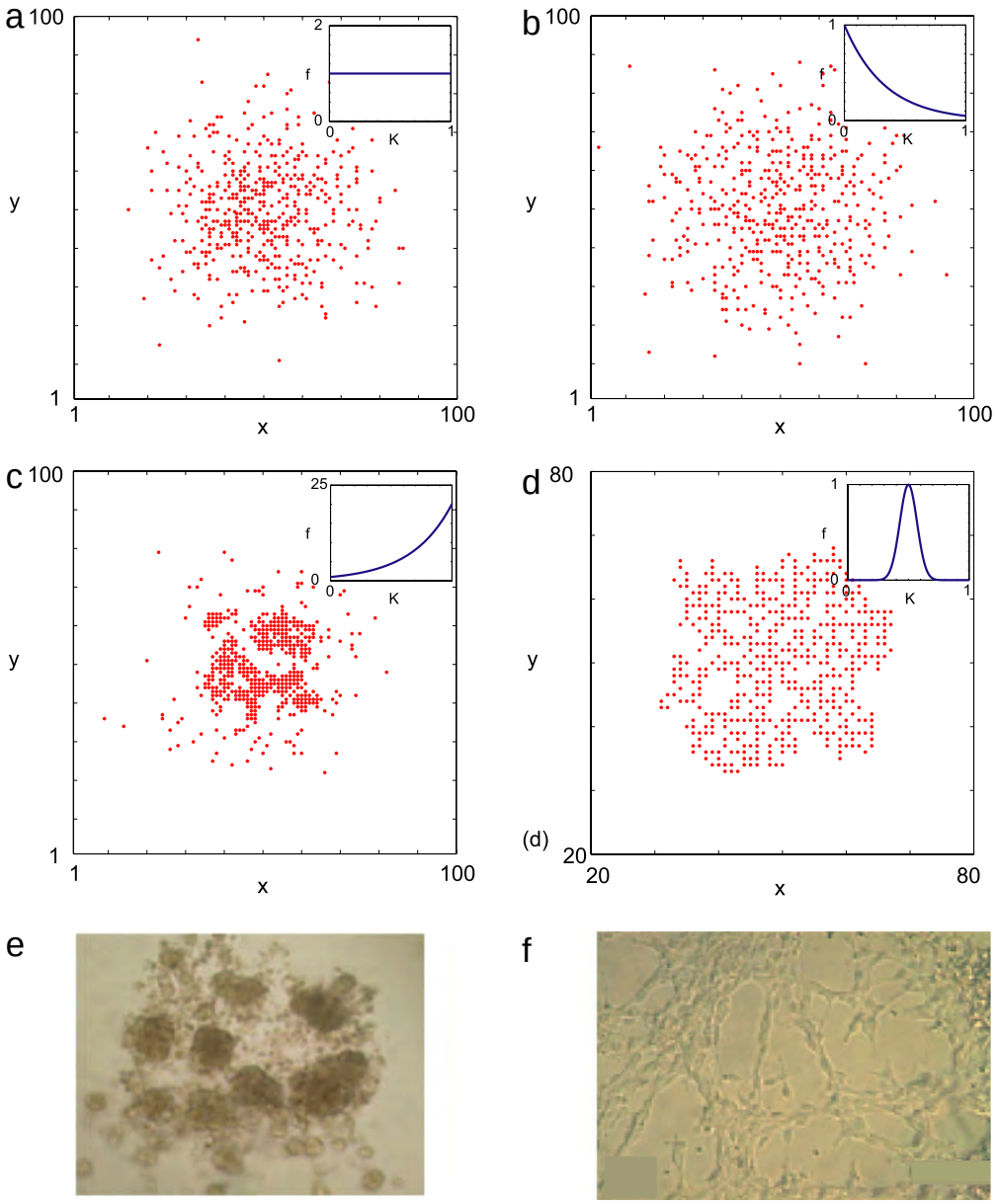

Fig. 2. Snapshots of discrete simulations where initially lattice sites $35 \leq i, j \leq 65$ are occupied with a probability 0.5. All simulations are performed with $P = \Delta = \tau = 1$, over 200 time steps. Snapshots of agent distributions are given for different binding functions: (a) $f(K) = 1$, (b) $f(K) = \mathrm{e}^{-3K}$, (c) $f(K) = \mathrm{e}^{3K}$, (d) $f(K) = \mathrm{e}^{-100(K-0.5)^2}$. Subfigure (d) is shown at a different scale to highlight the chain-like structure and lacunae mesoscale patterns. A plot of $f(K)$ is given as an inset in subfigures (a)–(d). Results from cell motility assays show (e) the formation of cell aggregates associated with the movement of ovarian cancer cells [5] (reproduced with permission from Neoplasia Press) and (f) the formation of chain-like structures associated with neural precursor cells grown as neurospheres [7] (reproduced with permission from the Company of Biologists).

which is the change in average occupancy of site $\mathbf{s}$ during the time interval from t to $t + \tau$ [15,18]:

$$\delta\langle C_{\mathbf{s}}\rangle = P(1 - \langle C_{\mathbf{s}}\rangle) \sum_{\mathbf{s}' \in \mathcal{N}\{\mathbf{s}\}} \langle C_{\mathbf{s}'}\rangle \frac{f(K_{\mathbf{s}})}{\sum_{\mathbf{s}'' \in \mathcal{N}\{\mathbf{s}'\}} f(K_{\mathbf{s}''})} - P\langle C_{\mathbf{s}}\rangle \sum_{\mathbf{s}' \in \mathcal{N}\{\mathbf{s}\}} (1 - \langle C_{\mathbf{s}'}\rangle) \frac{f(K_{\mathbf{s}'})}{\sum_{\mathbf{s}'' \in \mathcal{N}\{\mathbf{s}\}} f(K_{\mathbf{s}''})}. \tag{1}$$

The positive terms on the right of Eq. (1) represent the change in occupancy of site $\mathbf{s}$ due to transitions into site $\mathbf{s}$, while the negative terms represent the change in occupancy of site $\mathbf{s}$ owing to transitions out of site $\mathbf{s}$. The four factors in the second term can be interpreted as follows: (i) P is the probability that any agent is motile in the time interval of duration τ, (ii) $\langle C_{\mathbf{s}}\rangle$ is the probability that site $\mathbf{s}$ is occupied, (iii) $(1 - \langle C_{\mathbf{s}'}\rangle)$ is the probability that the target site $\mathbf{s}'$ is vacant, and (iv) $f(K_{\mathbf{s}'})/[\sum_{\mathbf{s}'' \in \mathcal{N}(\mathbf{s})} f(K_{\mathbf{s}''})]$ is a biasing factor that compares the binding function at the target site, relative to the sum of the binding functions at the $z_{\mathcal{N}}$ possible target sites. Since we interpret each of these factors as probabilities, this work assumes that the occupancy status of sites are independent [18]. Several previous investigations have also used this assumption and found it to be reasonable when considering averaged simulation data [15,17].

The discrete model is related to a PDE in the appropriate limit as $\Delta \to 0$ and $\tau \to 0$ and the discrete values of $\langle C_{\mathbf{s}} \rangle$ are written in terms of a continuous variable C. We now present the key steps connecting the discrete model with a continuum PDE. All terms in Eq. (1) are expanded in a Taylor series about a particular site, keeping terms up to $\mathcal{O}(\Delta^2)$. The resulting expression is divided by τ and we take limits as $\Delta \to 0$ and $\tau \to 0$ jointly, with the ratio Δ^2/τ held constant [29,30]. This gives a nonlinear diffusion equation which can be written as

$$\frac{\partial C}{\partial t} = D_0 \nabla \cdot [D(C) \nabla C]. \tag{2}$$

Here the free agent diffusivity is

$$D_0 = \frac{P}{2d} \lim_{\Delta,\tau \to 0} \left(\frac{\Delta^2}{\tau} \right), \tag{3}$$

where d is the dimension of the problem and the nonlinear diffusivity function is given by

$$D(C) = 1 - 2C(1 - C)\frac{f'(C)}{f(C)}. \tag{4}$$

This nonlinear diffusion model (Eqs. (2)–(4)) has this functional form for all periodic lattices. By way of illustration, the details of the Taylor series expansions connecting Eqs. (1) and (2) are given in the Appendix for the two-dimensional square lattice.

Making a connection between an exclusion process-based discrete motility mechanism and a nonlinear diffusion equation is novel. Although standard unbiased exclusion processes are an interacting particle system, surprisingly these models correspond to a linear diffusion mechanism. This occurs because all the individual agent–agent interactions are symmetric and do not appear in the continuum equations [15,18]. For the model presented here, we have introduced asymmetric interactions which appear in the corresponding PDE. This is similar to recent work by Deroulers et al. [17]. However we will show that the nonlinear diffusivity presented here gives far richer and more complex behavior.

If all assumptions made are reasonable, solutions of Eq. (2) should compare well with averaged simulation data. We might anticipate that if the binding function is chosen such that the magnitude of f' or f'' are sufficiently large, the truncated Taylor series used to connect the discrete and continuum models may be a poor approximation and the resulting continuum equations may be invalid. We will explore these issues with simulation data in Section 5. For the simple case that $f(K) = A$, for some constant A (Fig. 2(a)), all movements are independent of the coordination number of the target site and the discrete mechanism becomes an unbiased simple exclusion process. Under these conditions Eq. (2) becomes the linear diffusion equation which is known to match averaged simulation data very well [15,16].

In addition to developing a continuum PDE for the agent density, we also develop a continuum model to describe the evolution of the average position of an agent within the population. If site $\mathbf{s}$ is occupied, the expected displacement of the associated agent during the next time step is

$$\delta p_x = P \sum_{\mathbf{s}' \in \mathcal{N}\{\mathbf{s}\}} (1 - \langle C_{\mathbf{s}'} \rangle) \frac{f(K_{\mathbf{s}'})}{\sum_{\mathbf{s}'' \in \mathcal{N}\{\mathbf{s}\}} f(K_{\mathbf{s}''})} \widehat{\mathbf{x}} \cdot \mathbf{r}(\mathbf{s}', \mathbf{s}), \tag{5}$$

$$\delta p_y = P \sum_{\mathbf{s}' \in \mathcal{N}\{\mathbf{s}\}} (1 - \langle C_{\mathbf{s}'} \rangle) \frac{f(K_{\mathbf{s}'})}{\sum_{\mathbf{s}'' \in \mathcal{N}\{\mathbf{s}\}} f(K_{\mathbf{s}''})} \widehat{\mathbf{y}} \cdot \mathbf{r}(\mathbf{s}', \mathbf{s}), \tag{6}$$

where $\widehat{\mathbf{x}}$ and $\widehat{\mathbf{y}}$ are the horizontal and vertical unit direction vectors and $\mathbf{r}(\mathbf{s}', \mathbf{s})$ is the displacement vector of the target site $\mathbf{s}'$ relative to the original site $\mathbf{s}$. Dividing these expressions by τ, expanding all terms about $\mathbf{s}$, and holding Δ^2/τ finite, we let $\Delta \to 0$ and $\tau \to 0$ jointly giving

$$\frac{\mathrm{d}p_x}{\mathrm{d}t} = -2D_0 \frac{\partial C}{\partial x} \left[1 - (1 - C)\frac{f'(C)}{f(C)} \right], \tag{7}$$

$$\frac{\mathrm{d}p_y}{\mathrm{d}t} = -2D_0 \frac{\partial C}{\partial y} \left[1 - (1 - C)\frac{f'(C)}{f(C)} \right]. \tag{8}$$

The solution of these differential equations gives $p_x(t)$ and $p_y(t)$, which are the coordinates of the average trajectory of a tagged agent initially at position $(p_x(0), p_y(0))$. These trajectories are called pathlines because of the analogy with potential flow. For the case that $f(K) = A$, for some constant A, Eqs. (7) and (8) relax to previously described continuum models which are known to predict averaged simulation data accurately [16].

We now have three very different ways to view the exclusion process model. First, microscopic data from discrete simulations can be generated, visualized and analyzed in a variety of ways to demonstrate the broad range of mesoscale patterns that can be generated by this model. Second, simulation data from the discrete model can be averaged to describe the evolution of the agent density. This density data can then be compared with the solution of Eq. (2). Finally, pathline

data corresponding to a particular agent within the population can be generated and averaged. The evolution of the agent position within the population can then be compared with the solution of Eqs. (7)–(8).

We explore the regimes where the continuum models are valid and to assess whether particular mesoscale patterns appearing in the discrete simulations can be represented at the continuum level. Similarly, we investigate whether there is no continuum description for a particular range of mesoscale patterns.

5. Results

Simulation data will be generated and compared to the solution of the continuum models for two types of problems. First, we consider the evolution of an initially close-packed group of agents. Second, we consider the evolution of a uniformly seeded lattice for which, on average, there are no spatial gradients present initially in the system. These two problems demonstrate a wide range of behaviors supported by the discrete model and demonstrate the relationship between the discrete mechanism and the continuum models.

All PDE models are solved numerically using a finite difference approximation with constant grid spacing δx and implicit Euler stepping with constant time steps δt. Picard linearization is used to solve the resulting nonlinear systems.

5.1. Dispersing population

We consider a suite of simulations on a long narrow lattice of size 200×20. Periodic boundary conditions are imposed along the horizontal boundaries and reflecting boundary conditions are imposed on the vertical boundaries. All sites with $80 \leq i \leq 120$ are initially occupied. This configuration reduces the system to a one-dimensional problem, since there is no vertical structure imposed by the initial distribution of agents or the boundary conditions. Accordingly we compare the column density of agents, averaged over many simulations, with the numerical solution of a one-dimensional form of Eq. (2) [15,16]. For the pathline data, the horizontal position of the mth statistically identical realization of a tagged agent's trajectory, $x_m(t)$, is recorded. This data is averaged over M identically prepared realizations giving

$$\langle x(t)\rangle = \frac{1}{M}\sum_{m=1}^{M} x_m(t). \tag{9}$$

To compare the pathline data with the continuum predictions, we integrate Eq. (7) numerically and compare $p_x(t)$ with $\langle x(t)\rangle$ as considered by Simpson et al. [16]. Of course, different pathlines are obtained by placing the tagged agent in a different location. For this work we place the tagged agent at the edge of the dispersing population at (119, 10). Different results for the dispersing problem will now be presented and discussed for various $f(K)$.

5.1.1. Exponential binding function $f(K) = e^{AK}$

Setting $f(K) = e^{AK}$, the nonlinear diffusion function can be written as

$$D(C) = 1 - 2AC(1-C) = 1 - A/2 + 2A(C-1/2)^2. \tag{10}$$

Since we have $C \in [0, 1]$, specifying $A < 2$ leads to $D(C) > 0$ for all $C \in [0, 1]$. Alternatively, specifying $A > 2$ leads to $D(C) < 0$ for certain values of C.

To compare simulation data with the solution of the continuum models we first consider results with $A < 2$ where $D(C) > 0$. The three columns in Fig. 3 contain results for $A = 0, -1, -3$. Snapshots of the agents at $t = 0$ and 200 are given in rows (a)–(b), showing that the agents spread further as A decreases confirming that movements to lower coordination number target sites are favored as A decreases. The solution of Eq. (2) is compared with averaged column density profiles from the simulations in row (c), showing a good correspondence between the simulation data and the continuum model for $A = 0$ and $A = -1$. The density data for $A = -3$ begins to show a slight divergence between the simulation data and the continuum model.

Results in row (d) show that the average pathline data for the tagged agent compare well with the solution of Eq. (7) for all values of A. When $A = 0$, all movements are independent of the coordination number of the target site. The pathline starting at (119, 10) drifts to the right. This is consistent with Eq. (7) as $f'(K) = 0$ when $A = 0$, and $\partial C/\partial x < 0$ in this region, giving $\mathrm{d}p_x/\mathrm{d}t > 0$. As A is decreased, movements to sites with lower coordination numbers are favored. This means that the population tends to spread out faster than the $A = 0$ case. In row (d) we observe that the pathline starting at (119, 10) moves further to the right as A is decreased. This is intuitively reasonable.

The functional dependence of $D(C)$ is given in row (e). Clearly, when $A = 0$ we obtain a constant diffusivity and a linear diffusion equation, while as A decreases the diffusivity becomes nonlinear. In this case $D(C) > 0$ for all $C \in [0, 1]$. Under these conditions the solution of Eq. (2) is smooth, such as illustrated in row (c).

We point out that the comparison between the continuum models and the discrete data becomes less satisfactory as A is decreased below $A = -3$. Additional simulation data with $A < -3$ (not shown) confirms this, and this effect can be seen in the density data in row (c) for $A = -3$, where there is a minor disagreement between the simulation density data and the solution of (2) near the peak of the profile. This failure is due to the choice of the binding function. Choosing $A < -3$

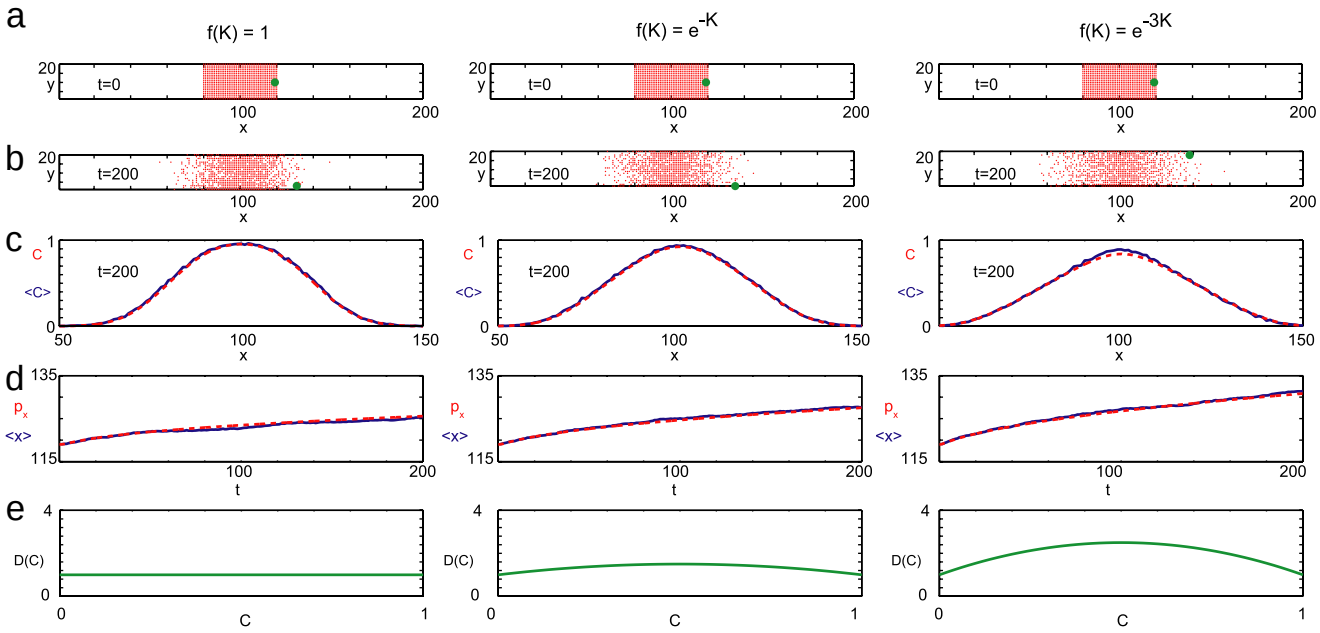

Fig. 3. Averaged agent density and pathline results with $f(K) = e^{AK}$ and $D(C) = 1 - A/2 + 2A(C - 1/2)^2$ for $A < 0$. Results are given for $A = 0, -1, -3$ in the three columns from left to right respectively. Snapshots of a single realization at $t = 0$ and 200 are given in rows (a) and (b), showing the distribution of a population of agents and the position of a tagged agent initially at (119, 10) (enlarged green bullet). Row (c) shows the averaged column density profiles $\langle C \rangle$ (solid blue) from the simulations compared with the continuum solution of Eq. (2) (dotted red). Row (d) compares the evolution of the mean horizontal position for the tagged agent (solid blue) with the continuum solution of Eq. (7) (dotted red). Row (e) shows the functional dependence of $D(C)$ on C. All simulation results are averaged over 100 Monte Carlo realizations with $P = \Delta = \tau = 1$. All continuum models are solved numerically with a spatial discretization $\delta x = 0.1$ and temporal discretization $\delta t = 0.005$. (For interpretation of the references to colour in this figure legend, the reader is referred to the web version of this article.)

means that the magnitude of f' and f'' are sufficiently large such that the truncated Taylor series, with finite Δ, are a poor approximation. This means that the continuum model may be invalid.

We also present and discuss simulation data and solutions of the continuum models for $f(K) = e^{AK}$ with $A > 0$. Physically, this means that movements to lattice sites with higher coordination numbers are favored. Under these conditions we expect the spreading of agents from the initial condition to be reduced relative to the $A = 0$ case. A transition is expected at $A = 2$, since $D(C) > 0$ when $A < 2$, while $D(C) < 0$ for some values of C when $A > 2$. Results in Fig. 4 illustrate these details for $A = 0, 1, 3$. Simulation data in rows (a)–(b) confirm that the spreading of agents is reduced as A increases. Averaged column density data from the simulations in row (c) is compared with the solution of Eq. (2). The comparison between the density data from the simulations and the solution of Eq. (2) is excellent for $A = 0$ and $A = 1$. The continuum density profiles for $A = 3$ contains shock discontinuities since $D(C) < 0$ for $C \in (1/2 - 1/(2\sqrt{3}), 1/2 + 1/(2\sqrt{3}))$ [19]. The comparison between the column density data and the solution of Eq. (2) is excellent when $A = 3$ provided that we are away from the location of the discontinuities. Alternatively, the comparison is less satisfactory near the discontinuities. This is because averaging simulation data across several identically prepared realizations smoothes the expected discontinuous profile.

A novel aspect of this work is that we relate an exclusion process to a PDE with discontinuous solutions. Other exclusion processes have also been linked to PDE models with discontinuous solutions, such as the totally asymmetric exclusion process [18,31,32] which is related to Burgers' equation [33]. The key difference between these two classes of models is that our work relates to a nonlinear diffusion model whereas the previous work relates to a nonlinear advection model.

The existence of discontinuous solutions of nonlinear diffusion equations has been previously analyzed [19] and these solutions are thought to play a role in infiltration [20]. More recently, Anguige and Schmeiser [14] proposed a continuous time master equation representing cell motility with adhesion and found that their discrete model was related to a nonlinear diffusion equation where the diffusivity could be negative. Other agent–agent binding rules in an exclusion process may also lead to nonlinear diffusion equations where the diffusivity can be negative [34].

The discontinuous solutions presented in the current work exist for problems where the initial data does not fall within the range of C where $D(C) < 0$. For example, the initial condition for the problem in Fig. 4 is such that $C(x, 0) = 1$ for $80 \leq x \leq 120$ while $C(x, 0) = 0$ elsewhere. These values of C only access the positive portion of the $D(C)$ curve when $A = 3$, as shown in row (e) of Fig. 4. The solution that evolves from this initial condition contains jump discontinuities across the region where $D(C) < 0$ [19], as illustrated in row (c). Had an alternative initial condition been chosen such that the initial distribution of $C(x, 0)$ been within the region where $D(C) < 0$, such as the discrete results shown in Fig. 2(c), then Eq. (2) would be ill-posed.

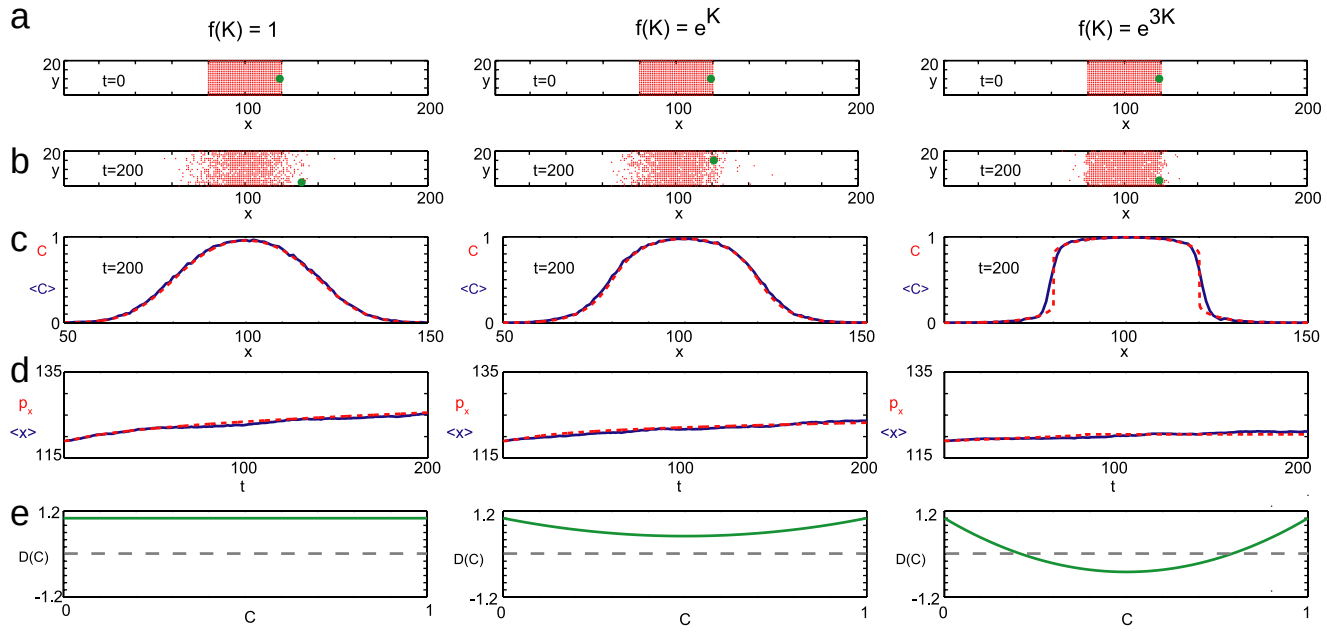

Fig. 4. Averaged agent density and pathline results with $f(K) = e^{AC}$ and $D(C) = 1 - A/2 + 2A(C - 1/2)^2$ for $A > 0$. Results are given for $A = 0$, 1, 3 in the three columns from left to right respectively. Snapshots of a single realization at $t = 0$ and 200 are given in rows (a) and (b), showing the distribution of a population of agents and the position of a tagged agent initially at (119, 10) (enlarged green bullet). Row (c) shows the averaged density profiles $\langle C \rangle$ (solid blue) extracted from the simulation data compared with the continuum solution of Eq. (2) (dotted red). Row (d) compares the evolution of the mean horizontal position for the tagged agent (solid blue) with the continuum solution of Eq. (7) (dotted red). Row (e) shows the functional dependence of $D(C)$ on C with the dashed horizontal line showing $D(C) = 0$. All simulation results are averaged over 100 Monte Carlo realizations with $P = \Delta = \tau = 1$. All continuum models are solved numerically with a spatial discretization $\delta x = 0.1$ and temporal discretization $\delta t = 0.005$. (For interpretation of the references to colour in this figure legend, the reader is referred to the web version of this article.)

Finally, pathline data in row (d) shows that, on average, the tagged agent drifts to the right for all values of A. However, we observe that the distance that the pathline drifts to the right decreases with A. This is reasonable since increasing A means that transitions to sites with high coordination numbers are favored and agents are more likely to stay close together. When $A = 3$ the agent–agent attraction is sufficiently strong so that, on average, the tagged agent remains almost stationary during the simulation. Since both the discrete and continuum pathlines hardly move at all, this gives the impression that the continuum and discrete models compare well for this case. In reality, we know from the density data in row (c) that the continuum–discrete comparison has already begun to break down near the discontinuities when $A = 3$.

5.1.2. Gaussian binding function $f(K) = e^{-A(K-B)^2}$

We now consider a Gaussian binding function that led to the formation of chain-like mesoscale patterns in Fig. 2. This binding function has a maximum at $K = B$, where B is a preferred coordination number. The steepness of the binding function is controlled by the parameter A. For this binding function we obtain

$$D(C) = 1 + 4AC(1 - C)(C - B). \tag{11}$$

Results are presented in Fig. 5 for $B = 0.5$ and $A = 1, 5, 10$. Results in the first column with $A = 1$ show a good correspondence between the simulation data and the continuum models for both the density and pathline data. For this choice of parameters $D(C) > 0$ and the solution of Eq. (2) is smooth. Results for $A = 5$ and $A = 10$ lead to the nonlinear diffusivity function becoming negative for some values of C, as shown in row (e). The solutions of Eq. (2) in these cases contain shock discontinuities.

As the value of A increases sufficiently, the match between the continuum and the discrete data becomes poor due to the increasing magnitude of f' and f''. We note that the original results in Fig. 1(d) that showed a strong chain-like mesoscale structure had a value of $A = 100$. This value is well beyond the range where the continuum approximation is valid and repeating the simulation data in Fig. 7 with $A = 100$ (not shown) reveals the formation of strong chain-like mesoscale structure but a very poor correspondence between the continuum and discrete data. This means that there is no continuum representation of the discrete model presented here with chain-like mesoscale structure. An important implication of this result is that it may be inappropriate to propose to represent systems with chain-like mesoscale structure with a continuum model.

The key feature of the Gaussian binding function that gives chain-like structures with lacunae is the presence of a local maximum in $f(K)$ combined with a sharp reduction in $f(K)$ either side of the maximum. Of course, other kinds of functions have similar properties. For example, we also experimented with a general logistic function of the form $f(K) = K^m(1 - K^n)$ or $f(K) = K^m(1 - K)^n$ with $m, n > 0$. Although these functions contain a maximum value we do not observe chains formation because they are less peaked than the Gaussian function.

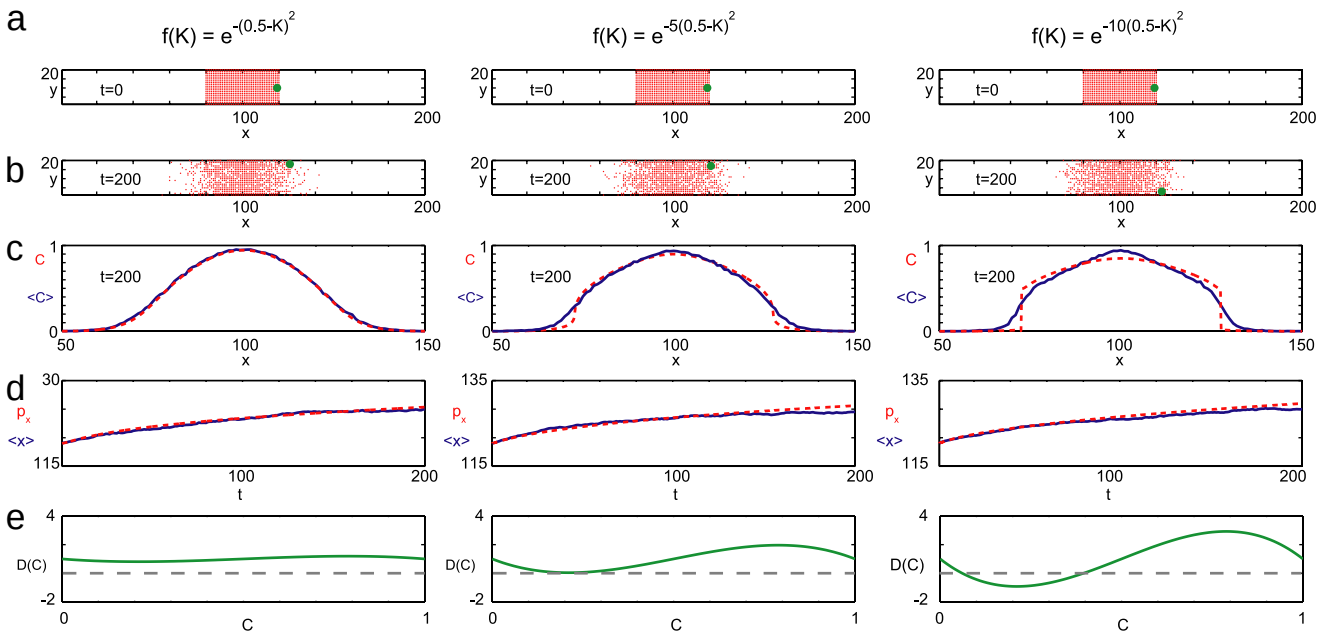

Fig. 5. Averaged agent density and pathline results with $f(K) = e^{-A(K-B)^2}$ and $D(C) = 1 + 4AC(1-C)(C-B)$. Results are given for $A = 1, 5, 10$ in the three columns from left to right respectively. Snapshots of a single realization at $t = 0$ and 200 are given in rows (a) and (b), showing the distribution of a population of agents and the position of a tagged agent initially at (119, 10) (enlarged green bullet). Row (c) shows the averaged density profiles $\langle C \rangle$ (solid blue) extracted from the simulation data compared with the continuum solution of Eq. (2) (dotted red). Row (d) compares the evolution of the mean horizontal position for the tagged agent (solid blue) with the continuum solution of Eq. (7) (dotted red). Row (e) shows the functional dependence of $D(C)$ on C with the dashed horizontal line showing $D(C) = 0$. All simulation results are averaged over 100 Monte Carlo realizations with $P = \Delta = \tau = 1$. All continuum models are solved numerically with a spatial discretization $\delta x = 0.1$ and temporal discretization $\delta t = 0.005$. (For interpretation of the references to colour in this figure legend, the reader is referred to the web version of this article.)

5.2. Aggregating population

Since the discrete model allows for movements that favor increasing an agent's coordination number, we expect that aggregation will be possible on a lattice that is randomly and uniformly seeded. Intuitively, we might expect that aggregation will occur when $f(K)$ is chosen with $f'(K) > 0$ so that transitions to sites with larger coordination numbers are favored. To test our intuition, a number of simulations on large uniformly seeded lattices with periodic boundary conditions were performed. Results in Fig. 6 show a single realization of two systems with $f(K) = e^{AK}$ and $A > 0$. Visual inspection of these simulation results illustrates that aggregates do not form when $A = 1$, while simulations with $A = 3$ lead to aggregation. Therefore, simply choosing $f(K)$ with $f'(K) > 0$ is insufficient to guarantee the formation of aggregates. Further simulations of the same problem on different sized lattices (50×50, 150×150) and over longer periods of time gave indistinguishable results.

Further understanding of aggregation formation is obtained by considering the steady state solution of Eq. (2) on an arbitrary domain with no flux boundary conditions. The steady state solution is $C(x, y) = C_0$, for some nonnegative constant C_0. To assess the stability of this steady state solution we perform a linear stability analysis by considering a small perturbation about the steady state given by

$$C = C_0 + \epsilon e^{(\sigma t + ik_x x + ik_y y)}, \tag{12}$$

where σ is the coefficient determining the stability of the steady state, k_x and k_y are the wavenumbers of the perturbation and $\epsilon \ll 1$. The dispersion relation is given by

$$\sigma = -D(C_0)(k_x^2 + k_y^2). \tag{13}$$

For stability we require $\mathrm{Re}(\sigma) < 0$, which is true provided $D(C_0) > 0$. Alternatively the steady state is unstable when $D(C_0) < 0$.

The transition from having positive diffusivity to negative diffusivity for $f(K) = e^{AK}$ occurs when $A = 2$. Therefore the results in Fig. 6 span this transition and explain the formation of aggregates when $A > 2$ whereas no aggregation occurs when $A < 2$. We repeated the simulations in Fig. 6 for the same $f(K)$ and different values of A to confirm that the transition to the formation of aggregates occurs when $A = 2$.

To quantify the transition to aggregation, we repeated the simulations in Fig. 6 and measured the size of clusters that form [35]. Several randomly occupied lattices, seeded well below the percolation threshold [36] were considered. The system is allowed to evolve with time and the size of clusters were counted over 40 Monte Carlo realizations for each initial condition. The mean cluster size and the variance of the cluster size are reported in Fig. 7. Results in the left column

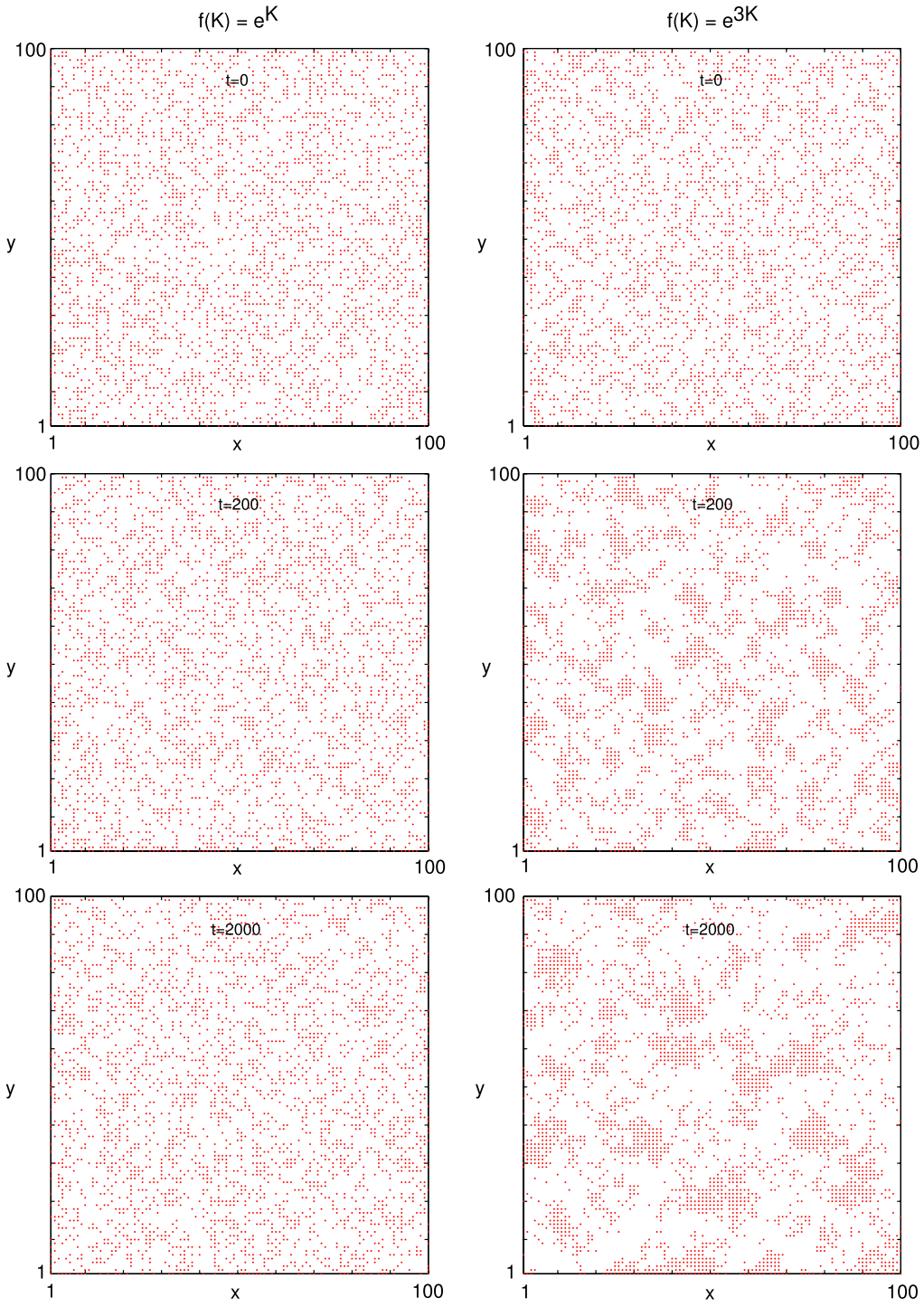

Fig. 6. Two potentially aggregation forming simulations on a 100×100 lattice, initially seeded uniformly with 30% occupancy. Periodic boundary conditions are imposed along all boundaries. Both simulations correspond to $f(K) = e^{AK}$ and snapshots are shown at $t = 0, 200, 2000$. Results in the left column ($A = 1$) do not aggregate whereas the right column ($A = 3$) form aggregates. All results correspond to $P = \Delta = \tau = 1$.

are for $f(K) = e^K$, which has $D(C) > 0$ for all C. The data shows a very small increase in the mean cluster size N and the variance σ over time. These increases are visually undetectable at the scale shown in Fig. 7. This small increase occurred for all values of the seeding density and confirms that no aggregation took place.

Results in the right column of Fig. 7 are for $f(K) = e^{3K}$, such that $D(C) < 0$ for some values of C. A large increase in the mean cluster size and variance with time is observed for the more densely occupied lattices. For the low density lattices the cluster size increases only modestly, whereas the average cluster size almost doubles on the high density lattices. We might expect from Fig. 7(b) that there would be no aggregation for low density lattices since $D(C) > 0$ when C is sufficiently small. This is not the case, as the stochastic nature of the random initial seeding and the randomness in the algorithm makes

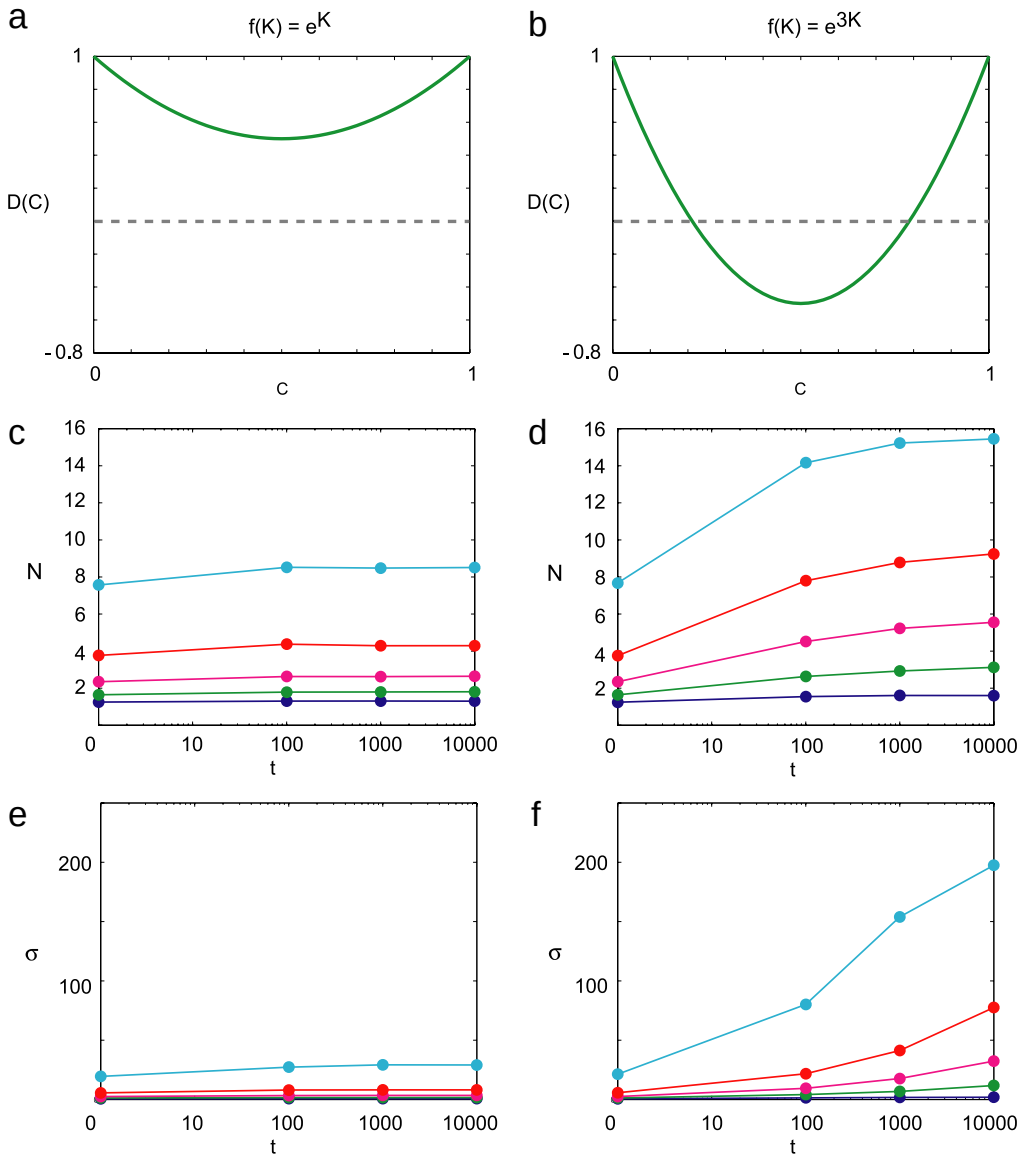

Fig. 7. The formation of aggregates is quantified by evaluating the mean cluster size N and the variance σ for a range of simulations on a square lattice that is initially uniformly occupied. Results are presented for $f(K) = e^{AK}$ for $A = 1$ (left column) and $A = 3$ (right column). Subfigures (a)–(b) show the nonlinear diffusivity functions with the horizontal line showing $D(C) = 0$. Results in (c)–(d) show the evolution of the averaged cluster size for uniformly seeded lattices with 10% (blue), 20% (green), 30% (magenta), 40% (red), 50% (cyan) occupancy. Profiles in (e)–(f) show the corresponding evolution of the variance. All simulations are for $P = \Delta = \tau = 1$ and the results are obtained by averaging over 40 Monte Carlo realizations. (For interpretation of the references to colour in this figure legend, the reader is referred to the web version of this article.)

it likely that, at some stage, $D(C) < 0$ in a localized region of the lattice, which leads to aggregations. This is why we see aggregation for all initial densities provided $f(K)$ is chosen so that $D(C) < 0$ for some values of C.

For the results in Fig. 7, the simulations are performed for up to 10 000 time steps, and our data indicates that this amount of time is sufficient for the system to approach a steady average cluster size. The simulations associated with the results in Fig. 7 were repeated several times on different sized lattices (50×50, 150×150) and the average cluster size and the variance were indistinguishable from those presented in Fig. 7.

The main difference between the two sets of simulation results in Fig. 7 is that we observe diffusive behavior when $A = 1$ and aggregation when $A = 3$. To confirm this transition we performed additional simulations to generate trajectory data from a tagged agent placed initially at the center of the uniformly occupied lattice. The evolution of the sum of the squared displacements of the tagged agent were recorded over many long simulations [10,30]. A range of problems were considered, and for all problems such that $D(C) > 0$ for all $C \in [0, 1]$ and the magnitude of f' and f'' sufficiently small, we observed that the sum of the squared displacements increased linearly with time. This confirms the diffusive nature of the motility mechanism. Alternatively, for problems where $D(C) < 0$ for certain values of C, the sum of the squared displacement of a tagged individual does not always increase linearly with time. This is because the tagged agent typically ends up trapped within a cluster of agents at some stage during the simulation.

6. Discussion and conclusion

We have presented and analyzed a discrete motility model capable of producing a range of mesoscale patterns. Our approach enables us to visualize discrete simulations, as well as relating our discrete model to continuum equations describing agent density and agent pathline data. Previous approaches to modeling mesoscale patterns have either taken a discrete or continuum approach separately [13,37,38], without any explicit connection between the two. The development and application of multiscale models is critical for understanding biological processes since biological data is also multiscale [39].

The discrete model is related to a nonlinear diffusion equation, and the solutions of this equation can either be smooth or discontinuous. Discontinuous solutions of the continuum model are obtained when $D(C)$ is negative for a range of C. Although previous theoretical studies [19] and some applications [14,20] have considered nonlinear diffusion equations with negative diffusion coefficients, we are unaware of any previous connection between exclusion processes and nonlinear diffusion equations which have discontinuous solutions.

It is interesting that the discrete and continuum models match for some parameters and fail to match for others. This transition confirms that the validity of our averaging arguments leading to the continuum model is parameter dependent. There are at least two possible explanations for the mismatch of the continuum and discrete models. First, our assumption of independence may be inappropriate in some scenarios. Second, for the dispersing population problem, we observed that the discrete and continuum models fail to match where the Taylor series approximations break down. This occurs when the magnitude of f' and/or f'' are sufficiently large. Consequently, if we were to observe a discrete system where the continuum approximation is invalid (Fig. 2(d)), blindly applying a continuum model to this system would be fraught with difficulties. Applying both the discrete and continuum descriptions using a multiscale model is a more comprehensive way to understand the validity of a continuum model.

Simulation data and analysis of the aggregating population problem confirms that the discrete motility mechanism can be used to model aggregation. We observe a transition between the presence and absence of aggregation patterns which is related to the sign of $D(C)$ in the continuum model. This indicates that nonlinear diffusion equations are related to aggregation, which is a very different way to model aggregation compared to other approaches [14,40–43].

Traditional modeling approaches assume that the transition to aggregation is analogous to phase separation in the Ising model for which the canonical treatment is to use a fourth order PDE model like the Cahn–Hilliard equation [14,41–43]. Our approach of relating a discrete motility mechanism to a nonlinear diffusion equation, and denoting the transition between stability (no aggregation) and instability (aggregation) where $D(C) = 0$ is very different. There are several practical differences between these two approaches. Our approach is simpler than using a fourth order PDE model from the point of view that we require fewer boundary conditions for the governing PDE and the issue of negative solutions does not arise with the second order PDE model. Furthermore, in addition to modeling aggregation patterns, our model is very flexible and can produce a range of mesoscale patterns that includes both aggregates and chain-like formations.

Acknowledgements

This work is supported by the Australian Research Council (ARC). Mat Simpson is an ARC Postdoctoral Fellow and Kerry Landman is an ARC Professorial Fellow. We thank Dr. Heather Young and Dr. Don Newgreen whose experimental work was the motivation for this paper.

Appendix. Taylor series

Our averaging arguments are valid for any periodic lattice and details of the series expansions depend on the structure of the lattice. Here we demonstrate how to expand some of the terms in Eq. (1) on the square lattice where sites are indexed as usual by integer coordinates, (i, j), corresponding to spatial positions $(i\Delta, j\Delta)$. As an example we now expand $\langle C_{i-1,j}\rangle$ and $f(\langle K_{i-1,j}\rangle)$ about site (i, j). For clarity we drop the angle brackets so that the expansion of $C_{i-1,j}$ is

$$C_{i-1,j} = C - \frac{\partial C}{\partial x}\Delta + \frac{\partial^2 C}{\partial x^2}\frac{\Delta^2}{2} + \mathcal{O}(\Delta^3), \tag{14}$$

where all terms on the right are evaluated at site (i, j). To obtain the series expansion of $f(K_{i-1,j})$, first we expand the argument and express the coordination number in terms of the site occupancy

$$\begin{aligned} K_{i-1,j} &= \frac{1}{8}\left(C_{i-2,j} + C_{i-2,j+1} + C_{i-1,j+1} + C_{i,j+1} + C_{i,j} + C_{i,j-1} + C_{i-1,j-1} + C_{i-2,j-1}\right), \\ &= C_{i-1,j} + \frac{3}{8}\left(\frac{\partial^2 C}{\partial x^2} + \frac{\partial^2 C}{\partial y^2}\right)_{i-1,j}\Delta^2 + \mathcal{O}(\Delta^3) \\ &= C - \frac{\partial C}{\partial x}\Delta + \frac{\partial^2 C}{\partial x^2}\frac{\Delta^2}{2} + \frac{3}{8}\left(\frac{\partial^2 C}{\partial x^2} + \frac{\partial^2 C}{\partial y^2}\right)\Delta^2 + \mathcal{O}(\Delta^3), \end{aligned} \tag{15}$$

where all terms in the expansion are evaluated at site (i, j). For ease of notation we rewrite Eq. (15) as

$$K_{i-1,j} = C + \overline{C}, \tag{16}$$

where $\overline{C}$ is a small perturbation. Expanding $f(K_{i-1,j})$ about (i, j) gives

$$f(K_{i-1,j}) = f(C + \overline{C}) = f(C) + f'(C)\overline{C} + f''(C)\frac{\overline{C}^2}{2} + \mathcal{O}(\Delta^3). \tag{17}$$

Eqs. (14) and (17) are examples of Taylor series expansions used to connect Eqs. (1) and (2) on a square lattice. The same kinds of expansions are also used to connect Eqs. (5)–(6) and (7)–(8).

Similar Taylor series expansions are relevant for other lattices. The main difference is that the constants multiplying the terms in the series depend on the lattice geometry.

It is possible to truncate the Taylor series expansions differently and allow higher order terms in the governing PDE model. This approach can yield fourth order PDE models [14,42,43]. Given that we have demonstrated that the second order PDE model developed here can predict the averaged discrete data accurately under a range of conditions, we have not pursued deriving higher order PDE models.

References

[1] P.K. Maini, D.L.S. McElwain, D. Levesley, Appl. Math. Lett. 17 (2004) 575–580.
[2] M.J. Simpson, D.C. Zhang, M. Mariani, K.A. Landman, D.F. Newgreen, Dev. Biol. 302 (2007) 553–568.
[3] M.A. Rivero, R.T. Tranquillo, H.M. Buettner, D.A. Lauffenburger, Chem. Eng. Sci. 44 (1989) 2881–2897.
[4] M. Ward, C. McCann, M. DeWulf, J.Y. Wu, Y. Rao, J. Neurosci. 23 (2003) 5170–5177.
[5] M.-L. Puiffe, C. Le Page, A. Filali-Mouhim, M. Zietarska, V. Ouellet, P.N. Toniny, M. Chevrette, D.M. Provencher, A.-M. Mes-Masson, Neoplasia 10 (2007) 820–829.
[6] N.B.E. Sawyer, L.K. Worrall, J.A. Crowe, S.L. Waters, K.M. Shakesheff, F.R.A.J. Rose, S.P. Morgan, Biotechnol. Bioeng. 100 (2007) 159–167.
[7] T.S. Jacques, J.B. Relvas, S. Nishimura, R. Pytela, G.M. Edwards, C.H. Streuli, C. Ffrench-Constant, Development 125 (1998) 3167–3177.
[8] H.M. Young, A.J. Bergner, R.B. Anderson, H. Enomoto, J. Milbrandt, D.F. Newgreen, P.M. Whitington, Dev. Biol. 270 (2004) 455–473.
[9] E.L. Bearer, J.S. Lowengrub, H.B. Frieboes, Y.L. Chuang, F. Jin, S.M. Wise, M. Ferrari, D.B. Agus, V. Cristini, Cancer Res. 69 (2009) 4493–4501.
[10] M.J. Simpson, A. Merrifield, K.A. Landman, B.D. Hughes, Phys. Rev. E 76 (2007) 021918.
[11] H.G. Othmer, A. Stevens, SIAM. J. Appl. Math. 57 (4) (1997) 1044–1081.
[12] K.J. Painter, J.A. Sherratt, J. Theoret. Biol. 225 (2003) 327–339.
[13] K.J. Painter, Bull. Math. Biol. 71 (2009) 1117–1147.
[14] K. Anguige, C. Schmeiser, J. Math. Biol. 58 (2009) 395–427.
[15] M.J. Simpson, K.A. Landman, B.D. Hughes, Physica A 388 (2009) 399–406.
[16] M.J. Simpson, K.A. Landman, B.D. Hughes, Phys. Rev. E 79 (2009) 031920.
[17] C. Deroulers, M. Aubert, M. Badoual, B. Grammaticos, Phys. Rev. E 79 (2009) 031917.
[18] T.M. Liggett, Stochastic Interacting Systems: Contact, Voter and Exclusion Processes, Springer-Verlag, Berlin, 1999.
[19] T.P. Witelski, Appl. Math. Lett. 8 (1995) 27–32.
[20] D.A. DiCarlo, R. Juanes, T. LaForce, T.P. Witelski, Water Resour. Res. 44 (2008) W02406.
[21] K. Hollig, Trans. Amer. Math. Soc. 278 (1983) 299–316.
[22] M. Burd, Physica A 372 (2006) 124–131.
[23] T.S. Deisboeck, I.D. Couzin, BioEssays 31 (2009) 190–197.
[24] W.G. Weng, T. Chen, H.Y. Yuan, W.C. Fan, Phys. Rev. E 74 (2006) 036102.
[25] J.M. Ziman, Models of Disorder, Cambridge University Press, 1979.
[26] F. Spitzer, Adv. Math. 5 (1970) 256–290.
[27] D. Chowdhury, A. Schadschneider, K. Nishinari, Phys. Life Rev. 2 (2005) 318–352.
[28] N.R. Druckenbrod, M.L. Epstein, Dev. Dyn. 236 (2007) 84–92.
[29] E.A. Codling, M.J. Plank, S. Benhamou, J. R. Soc. Interface 5 (2008) 813–834.
[30] B.D. Hughes, Random Walks and Random Environments, vol. 1, Oxford University Press, Oxford, UK, 1995.
[31] G.M. Schütz, J. Stat. Phys. 88 (1997) 427–445.
[32] A. Schadschneider, Physica A 313 (2002) 153–187.
[33] G.B. Whitham, Linear and Nonlinear Waves, Wiley, New York, 1974.
[34] A.E. Fernando, K.A. Landman, M.J. Simpson, Phys. Rev. E (2010) (in press).
[35] J. Hoshen, R. Kopelman, Phys. Rev. B 14 (1976) 3438–3444.
[36] B.D. Hughes, Random Walks and Random Environments, vol. 2, Oxford University Press, Oxford, UK, 1995.
[37] R.M.H. Merks, E.D. Perryn, A. Shirinifard, J.A. Glazier, PLoS Comput. Biol. 4 (2008) 1–16.
[38] L.M. Sander, T.S. Deisboeck, Phys. Rev. E 66 (2002) 051901.
[39] B.C. Thorne, A.M. Bailey, D.W. DeSimone, S.M. Peirce, Birth Defects Res. C 81 (2007) 344–353.
[40] N.J. Armstrong, K.J. Painter, J.A. Sherratt, J. Theoret. Biol. 243 (2006) 98–113.
[41] T. Callaghan, E. Khain, L.M. Sander, R.M. Ziff, J. Stat. Phys. 122 (5) (2006) 909–923.
[42] E. Khain, L.M. Sander, Phys. Rev. E 77 (2008) 051129.
[43] S.M. Wise, J.S. Lowengrub, H.B. Frieboes, V. Cristini, J. Theoret. Biol. 253 (2008) 524–543.